

Nuclear saturation in lowest-order Brueckner theory with two- and three-nucleon forces in view of chiral effective field theory

M. Kohno*

Research Center for Nuclear Physics, Osaka University, Ibaraki 567-0047, Japan

The nuclear saturation mechanism is discussed in terms of two-nucleon and three-nucleon interactions in chiral effective field theory (Ch-EFT), using the framework of lowest-order Brueckner theory. After the Coester band, which is observed in calculating saturation points with various nucleon-nucleon (NN) forces, is revisited using modern NN potentials and their low-momentum equivalent interactions, detailed account of the saturation curve of the Ch-EFT interaction is presented. The three-nucleon force (3NF) is treated by reducing it to an effective two-body interaction by folding the third nucleon degrees of freedom. Uncertainties due to the choice of the 3NF low-energy constants c_D and c_E are discussed. The reduction of the cutoff-energy dependence of the NN potential is explained by demonstrating the effect of the 3NF in the 1S_0 and 3S_1 states.

I. INTRODUCTION

It is one of the fundamental problems in nuclear physics to understand saturation properties of atomic nuclei on the basis of the underlying interactions between nucleons. A description of the nucleon-nucleon (NN) interaction has been developed in about eighty years after the meson theory was conjectured by Yukawa in 1935 [1]. It was recognized in the early stage from the analyses of NN scattering data that the NN force described as an instantaneous two-nucleon potential is strongly repulsive at short distances as is fairly well approximated by a hard core. On the other hand, experimental evidences that disclose single-particle structures of atomic nuclei have been accumulated. An explanation of this seemingly contradicting situation was given by Brueckner theory in the 1950's [2]. The central element in this theory is a reaction matrix (or G matrix), which describes in-medium NN correlation and takes care of strong repulsion of the NN interaction at short distances. Afterwards, the theory was organized as the quantum many-body theory [3–5]: the framework of a perturbation description of nuclei in terms of the G -matrices.

Although the Brueckner theory was successful to qualitatively account for the reason for the appearance of the shell structure, a quantitative explanation of nuclear saturation properties has not been completed. Various calculations in nuclear matter showed that theoretical saturation points obtained from existing NN potentials which achieve very high accuracy in describing scattering data miss the empirical location [6, 7]. It is improbable that a certain new functional form of the potential, either in coordinate space or in momentum space, resolves the problem. Concerning higher-order correlations not included in these nuclear matter calculations, their contributions have been shown to be rather modest and do not improve the situation [8]. In addition, different quantum many-body frameworks, for example a variational method, also predict similar saturation properties to those in the Brueckner theory [9, 10].

There have been various conjectures about the missing mechanism to explain the correct nuclear saturation properties, such as relativistic effects, many-body forces, and possible modifications of nucleon properties in the nuclear medium. Among them, the three-nucleon force (3NF) contribution is a promising candidate to be investigated first, for which the Fujita-Miyazawa [11] type interaction involving an isobar Δ excitation is a prototype. As for the relativistic effect, Dirac-Brueckner calculations were shown to explain quantitatively nuclear matter saturation [12]. However, the processes including anti-nucleon excitations involve considerably higher energy scale than that of the isobar Δ excitation. Thus, it is important to establish the contribution of the three-nucleon force effects to examine if it is reasonable or not. There have been many attempts in the literature to use the 3NF contributions to reproduce correct nuclear saturation properties [10, 13–16]. However, these calculations are exploratory or include more or less phenomenological adjustments.

The situation has changed since the description of the NN interaction in chiral effective field theory (Ch-EFT) [17, 18] achieved, at the N^3 LO level, the comparable accuracy with other modern NN interactions below the pion production threshold energy and the 3NFs were introduced systematically and consistently to the NN sector. The study of Ch-EFT 3NF contributions in nuclear and neutron matter started in the many-body framework such as the Hartree-Fock approximation [19], and perturbation calculations up to the second order [20] and the third order [21, 22].

* kohno@rcnp.osaka-u.ac.jp

The present author gave a brief report, in Ref. [23], on the lowest-order Brueckner theory (LOBT) calculations in nuclear matter using the $N^3\text{LO}$ NN and NNLO 3NF interactions, in which a focus was put on the effective spin-orbit strength. The 3NF was treated as a density-dependent effective NN force, as in Holt *et al.* [24] but without introducing an approximation for off-diagonal matrix elements. More details about the calculated saturation curves were presented in Ref. [25]. Sammarruca *et al.* [26] presented results of similar LOBT calculations. They also discuss cutoff scale dependence and order-by-order convergence of the Ch-EFT interactions on nuclear and neutron matter calculations [27]. Carbone *et al.* [28, 29] have investigated the Ch-EFT 3NF contributions in their self-consistent Green's function formalism, taking into account a correlated average of the 3NF over the third nucleon. All these calculations find the important and desirable effects of the 3NF to improve the description of nuclear saturation properties.

It was shown in Ref. [25] that the saturation curve becomes close to the empirical one when the effects of the 3NF are included as an effective NN interaction by folding the third nucleon. In addition, the strong spin-orbit strength required for nuclear mean field calculations is explained by the additional contribution from the 3NF [23, 25]. A further interesting observation is that the cutoff-energy dependence was substantially reduced by the inclusion of the 3NF effects, which is a desirable feature for the effective theory having a cutoff parameter. The mechanism to produce these results was briefly discussed in Ref. [25]. This paper supplements the explanation by extending the discussion to the wide scope of the nuclear saturation mechanism.

In fermion many-body calculations, a Pauli exclusion plays essential roles in considering two-particle correlations. In a nucleon-nucleon correlation in the nuclear medium, the Pauli effect reveals dominantly in the triplet even channel, because typical momentum transfer in the tensor correlation lies in the momentum region of the Fermi momentum of nuclei. On the other hand, short-range repulsion is characterized by higher momentum transfer, and hence the short-range correlation is not sensitive to the Pauli effect. The introduction of equivalent interactions in low-momentum space [30] is concerned with the elimination of the short-range and thus high-momentum component of the NN interaction in the two-nucleon sector. It is useful to consider nuclear matter saturation curves obtained using low-momentum equivalent interaction. Because the tensor interaction is also transformed to fit in the low-momentum space, the saturation curve varies with changing the low-momentum scale. This variation is due to the elimination of possible correlations in the many-body space, which should be recovered by inducing many-body effective interactions in the restricted space. This situation is shown to be analogous to the 3NF effects.

Section 2 revisits a Coester band of LOBT nuclear matter calculations, which was first demonstrated by Coester *et al.* [31] in 1970. The character of unitary uncertainties in the NN potential on the LOBT calculation is further demonstrated in Sect. 3 by using low-momentum interaction, which is equivalent to the original interaction in the low-momentum two-body space. Section 4 reports the results of the nuclear matter calculations by using Ch-EFT interactions. First, uncertainties due to the 3NF parameters c_D and c_E are discussed in subsection 4.1. It is shown that the c_D and c_E term contributions to nuclear matter energies cancel each other when $c_D \approx 4c_E$ is satisfied, and this relation is favorable to describe nuclear saturation properties as shown in Ref. [25]. On the basis of this observation, the results with $c_D = c_E = 0$ are first presented and the dependence of calculated energies on c_D and c_E is demonstrated. Qualitative explanations of the 3NF contributions are given in Section 5. Summary and some remarks follow in Sec. 6.

II. COESTER BAND OF LOBT SATURATION POINTS

The Coester band of LOBT nuclear matter calculations is recapitulated in order to give the basis for the discussion in the following sections.

In the lowest-order of the Brueckner-Bethe-Goldstone many-body theory, the energy per nucleon in nuclear matter with the Fermi momentum k_F is given by

$$E/A = \frac{1}{\rho} \sum_{|\mathbf{k}| \leq k_F} \frac{\hbar^2}{2m} k^2 + \frac{1}{2\rho} \sum_{|\mathbf{k}_1|, |\mathbf{k}_2| \leq k_F} \langle \mathbf{k}_1 \mathbf{k}_2 | G | \mathbf{k}_1 \mathbf{k}_2 \rangle_A, \quad (1)$$

where spin and isospin summations are implicit and the subscript A stands for the antisymmetrization. The nucleon density of symmetric nuclear matter is calculated as $\rho = \sum_{|\mathbf{k}| \leq k_F} 1 = \frac{2k_F^3}{3\pi^2}$. The reaction matrix G is

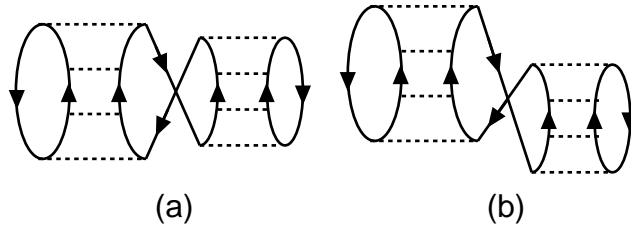


FIG. 1: Three-hole line diagrams corresponding to the definition of single-particle potential, Eq. (3). The downwards (upwards) arrow represents an occupied (unoccupied) state. The dotted line denotes a bare interaction V .

determined by the G -matrix equation

$$G|\mathbf{k}_1\mathbf{k}_2\rangle_A = V|\mathbf{k}_1\mathbf{k}_2\rangle_A + \sum_{\mathbf{k}'_1\mathbf{k}'_2} V|\mathbf{k}'_1\mathbf{k}'_2\rangle_A \langle\mathbf{k}'_1\mathbf{k}'_2| \frac{Q}{e(k_1) + e(k_2) - e(k'_1) - e(k'_2)} |\mathbf{k}'_1\mathbf{k}'_2\rangle_A \langle\mathbf{k}'_1\mathbf{k}'_2| G|\mathbf{k}_1\mathbf{k}_2\rangle_A, \quad (2)$$

where V denotes a two-nucleon bare interaction. The single-particle energy $e(k)$ of an occupied state, $k \leq k_F$, is determined from the G -matrix self-consistently:

$$e(k) = \frac{\hbar^2}{2m}k^2 + \sum_{|\mathbf{k}'| \leq k_F} \langle\mathbf{k}\mathbf{k}'| G|\mathbf{k}\mathbf{k}'\rangle_A. \quad (3)$$

This definition corresponds to including diagrams shown in Fig. 1 in the energy. As for the unoccupied state, there are some ambiguities linked to the choice of intermediate spectra of the perturbative expansion. There are two standard prescriptions. The gap choice takes $e(k) = \frac{\hbar^2}{2m}k^2$ for $k > k_F$. The reason for this prescription is that the insertion for the particle state should be treated as the three-body correlation diagrams and the net contribution of these diagrams is small. The other is the continuous choice; that is, $e(k) = \frac{\hbar^2}{2m}k^2 + \sum_{|\mathbf{k}'| \leq k_F} \langle\mathbf{k}\mathbf{k}'| G|\mathbf{k}\mathbf{k}'\rangle_A$ for $k > k_F$. In this case, there is no rigorous correspondence similar to that in Fig. 1, because G -matrix cannot be on-shell for the insertion in the perturbative expansion of the total energy. Since Song *et al.* [8] showed that the net contribution in the total energy from higher-order diagrams is smaller in the continuous prescription, this choice has been commonly employed. In the calculations below, the Pauli exclusion operator is approximated by introducing angle-averaging. The accuracy of this approximation in Ref. [32, 33] for the gap prescription. The denominator of Eq. (2) is also treated with an angle-average for \mathbf{k}'_1 and \mathbf{k}'_2 .

Nuclear matter calculations in the LOBT have shown [6, 7] that varying nucleon-nucleon potentials predict different saturation curves; namely, the relation of the calculated energy per nucleon E/A to the Fermi momentum of nuclear matter k_F . The salient feature is that the saturation point of the different interaction, the minimum of the saturation-energy curve, lies in a rather narrow band, in which the empirical saturation point does not locate. This band has been called as the Coester band, after Coester *et al.* presented such systematic results in Ref. [31]. This property persists in the calculations using modern nucleon-nucleon potentials with higher accuracy in reproducing NN scattering data. Various calculations in the literature indicate that higher-order correlations beyond the standard Brueckner calculation do not change the situation, although a different choice of the intermediate spectra of the propagator in the G -matrix equation causes a shift of the Coester band itself. Figure 2 demonstrates saturation curves obtained in the LOBT with the continuous (thick curves) and gap (thin curves) prescriptions for the intermediate spectra of the propagator in the G -matrix equation, using NN potentials such as AV18 [34], NSC97 [35], CD-Bonn [36], and fss2 [37].

TABLE I: Deuteron D -state probability p_D of the NN interactions used in Fig. 2.

	AV18	NSC97	fss2	CD-Bonn
p_D	5.76	5.39	5.49	4.85

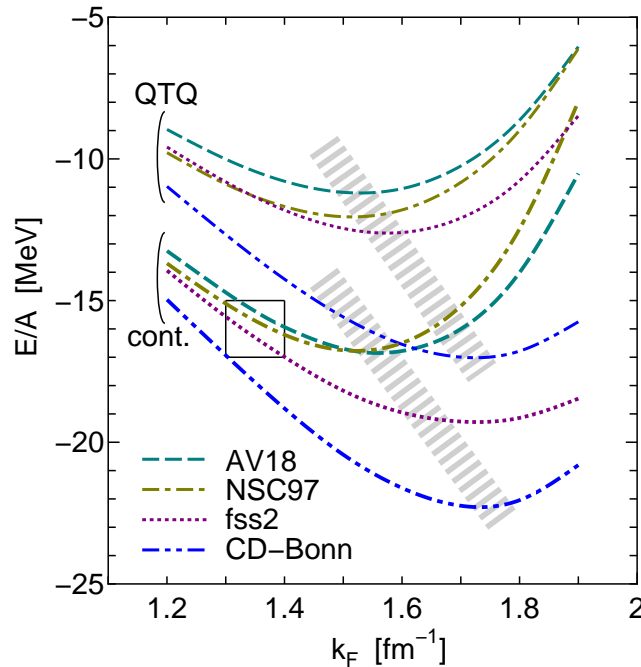


FIG. 2: LOBT saturation curves in symmetric nuclear matter with the continuous (thick curves) and the gap (thin curves) prescriptions for the intermediate spectra, using modern NN potentials: AV18 [34], NSC97 [35], CD-Bonn [36], and fss2 [37]. Two broad hatches are a rough guide for the Coester band. The standard empirical saturation point is indicated by the square.

The variation of the saturation curve is known to be controlled by the strength of the tensor component. Because the considerable attraction in the proton-neutron (3S_1) channel is brought about by ladder correlation through the tensor force and the correlation is influenced by the Pauli effect in the nuclear medium, the binding energy of nuclear matter depends on the weight of the tensor component of the NN potential used. A useful measure to specify the strength of the tensor correlation is a deuteron D -state probability p_D , although this quantity is not measurable. Table 1 tabulates values of p_D of the NN interactions used in Fig. 2.

The NN potential with larger p_D , which provides attractive contribution by the tensor correlation in free space, tends to give a shallower saturation curve in nuclear matter due to the suppression of the tensor correlation. Although this qualitative expectation does not explain why the shift due to the difference of p_D moves in the narrow Coester band, it is apparent that we should expect the variation of the saturation point depending on the NN potential used in many-body calculations.

It is worthwhile to note that most of saturation curves calculated with the continuous prescription go past near the empirical saturation point which is indicated by the square in Fig. 2. It implies that the G -matrices as an effective interaction quantitatively work well for describing various structural and scattering properties of nuclei, as far as the quantities associated with the slope and/or the curvature of the saturation curve are not crucial for them.

III. LOBT CALCULATIONS USING LOW-MOMENTUM INTERACTIONS

A different approach to manipulate the singular short-range part of the NN force was developed in the 1990's: that is, low-momentum interaction theory [30]. The method is based on a renormalization group viewpoint and equivalent interaction theory in a restricted space. Starting from the bare NN interaction, high-momentum components are integrated out to define the interaction V_{lowk} in low-momentum space appropriate for low-energy nuclear physics. V_{lowk} is the interaction which reproduce the same half-on-shell T matrices of the original bare NN interaction V . Denoting the projection operator into the low-momentum space by P , V_{lowk} is defined to satisfy

$$PTP = PV_{lowk}P + PV_{lowk}P \frac{1}{\omega - t} PTP, \quad (4)$$

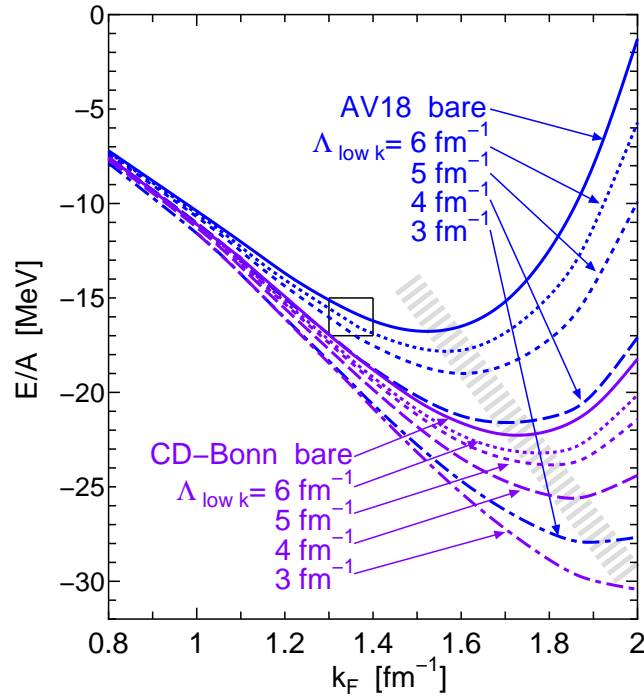


FIG. 3: Variation of LOBT saturation curves in symmetric nuclear matter under the change of a low-momentum cutoff scale $\Lambda_{low k}$. Results for two NN potentials, AV18 [34] and CD-Bonn [36], are shown. The broad hatch is a rough guide for the band in which saturation minima locate.

where $\frac{1}{\omega-t}$ is a free nucleon propagator and T -matrix is given by $T = V + V \frac{1}{\omega-t} T$ in the entire space.

It is straightforward to do nuclear matter LOBT calculations by taking the low-momentum interaction as the input NN interaction. Because high-momentum components are eliminated, the G -matrix equation is not meant for taking care of them, but the G -matrix equation and the self-consistency of single-particle energies take into account ladder correlations together with certain higher order correlations in the low-momentum space. By definition, low-momentum interaction is regarded as obtained by a unitary transformation, because low-momentum interaction in the Lee-Suzuki method [38, 39] is identical to that of the renormalization group consideration [30]. In this sense, the low-momentum interaction is a soft version of the original bare interaction by some appropriate unitary transformation. Thus we expect that the saturation point obtained by $V_{low k}$ with a different low-momentum scale moves in the Coester band. As an illustration, the AV18 [34] and CD-Bonn [36] potentials [34, 36] are taken as a starting bare potential and construct low-momentum interaction for the cutoff of $\Lambda_{low k} = 6, 5, 4$, and 3 fm^{-1} , respectively. The saturation curves obtained in the LOBT with these potentials are plotted in Fig. 3. Varying the low-momentum cutoff $\Lambda_{low k}$, the saturation point systematically shifts on the Coester band. The similar result was presented before by Kuckei *et al.* [40]. The difference of the saturation curves obtained from the AV18 and CD-Bonn is seen to gradually reduce by lowering the low-momentum scale $\Lambda_{low k}$.

The unitary transformation of the NN interaction preserves corresponding on-shell properties of the original interaction in the low-momentum space. However, it induces many-body interactions when practiced in a many-body space. If these induced many-body interactions are included, the result of the original bare interaction should be recovered. The occurrence of this restoration was actually demonstrated in few-body calculations in the similarity renormalization group method [41]. In the case of low-momentum interaction method, the unitary transformation to the low-momentum space is to be carried out in the many-body space. Such a framework to include the induced interaction was developed by Suzuki, Okamoto, and Kumagai [42] as the unitary-model-operator-method (UMOA), and was applied for ^{16}O and ^{40}Ca in [43]. However, an explicit application of this method in nuclear matter has not been undertaken. The inclusion of higher-order correlations are beyond the scope of the present paper.

The necessity of incorporating the induced many-body interaction to recover the result of the original bare force is analogous to the introduction of the 3NF and the cutoff-scale dependence of its contributions. This point is discussed in the following sections.

IV. LOBT CALCULATIONS WITH THE N³LO NN INTERACTIONS IN CHIRAL EFFECTIVE FIELD THEORY

This section supplements the results of Ref. [25], where LOBT nuclear matter calculations are presented, using NN and 3N forces in chiral effective field theory. The NNLO 3NF has 5 low-energy constants. Three of them are fixed in the NN sector: $c_1 = -0.81 \text{ GeV}^{-1}$, $c_3 = -3.4 \text{ GeV}^{-1}$, and $c_4 = 3.4 \text{ GeV}^{-1}$ [44]. Remaining parameters, c_D and c_E , are adjusted to reproduce, for example, observables of few-nucleon systems. In Ref. [25], the values of $c_D = -4.381$ and $c_E = -1.126$ given in the Table 1 of the paper by Hebeler *et al.* [21] for the EGM interaction [44] were employed, and uncertainties due to c_D and c_E were disregarded because the nuclear matter saturation curves are reasonably well reproduced. In this paper, a more careful analysis is prepared for the uncertainties on these constants. Using a Hartree-Fock level expression, it is shown that if the relation of $c_D \approx 4c_E$ is satisfied, contributions of these two terms almost cancel each other. The values used in Ref. [25] approximately fulfil this relation. It indicates that the condition of $c_D \approx 4c_E$ is preferable for the LOBT calculations in nuclear matter. It is interesting that the few-nucleon calculations [45] actually suggests $c_D \approx 4c_E$ in the case of $c_D < 0$ in its continuous uncertainties. Therefore, in this paper, calculated results with $c_D = c_E = 0$ are first presented as a reference case and the variation due to changing c_D and c_E is shown.

A. Uncertainties of c_D and c_E

Before carrying out explicit G -matrix calculations in nuclear matter, it is instructive to consider the mean-field contributions of the c_D and c_E terms to the nuclear matter energy. Integrating three-nucleon matrix elements in symmetric nuclear matter, we obtain the following expression for the contributions to the energy, which are same as those given by Bogner *et al.* in Ref. [19].

$$E_{c_D}/A = -\frac{3^5}{4(2\pi)^4} \frac{1}{k_F^3} \frac{g_A c_D}{f_\pi^4 \Lambda_\chi} \int_0^{k_F} Y^2 dY \int_0^{\sqrt{k_F^2 - Y^2}} p^2 dp \int_0^{\frac{2}{3}(k_F + Y)} q^2 dq \times \frac{4p^2}{4p^2 + m_\pi^2} f_R^2(p, q) F(p, Y; k_F) G(q, Y; k_F), \quad (5)$$

$$E_{c_E}/A = -\frac{3^5}{(2\pi)^4} \frac{1}{k_F^3} \frac{c_E}{f_\pi^4 \Lambda_\chi} \int_0^{k_F} Y^2 dY \int_0^{\sqrt{k_F^2 - Y^2}} p^2 dp \int_0^{\frac{2}{3}(k_F + Y)} q^2 dq \times f_R^2(p, q) F(p, Y; k_F) G(q, Y; k_F), \quad (6)$$

where $f_R = \exp\{-(p^2 + \frac{3}{4}q^2)/\Lambda_{3NF}^4\}$ is a regularization factor and two functions $F(p, Y; k_F)$ and $G(q, Y; k_F)$ are defined as

$$F(p, Y; k_F) = \begin{cases} 2 & \text{for } p \leq k_F - Y, \\ \frac{k_F^2 - p^2 - Y^2}{Yp} & \text{for } k_F - Y \leq p \leq \sqrt{k_F^2 - Y^2}. \end{cases} \quad (7)$$

$$G(q, Y; k_F) = \begin{cases} 2 & \text{for } 0 \leq q \leq \frac{2}{3}(k_F - Y), \\ \frac{k_F^2 - (\frac{3}{2}q - Y)^2}{3Yq} & \text{for } \frac{2}{3}(k_F - Y) \leq q \leq \frac{2}{3}(k_F + Y). \end{cases} \quad (8)$$

Numerical calculations in the range of $0.8 \leq k_F \leq 1.8 \text{ fm}^{-1}$ with $f_\pi = 92.4 \text{ MeV}$, $\Lambda_\chi = 700 \text{ MeV}$, and $\Lambda_{3NF} = 2 \text{ fm}^{-1}$ show that the values of E_{c_D}/A and E_{c_E}/A is fitted well by simple quadratic polynomials of the function of the density $\rho = \frac{2k_F^3}{3\pi^2}$ as

$$\frac{E_{c_D}(\rho)}{A} = c_D \times (-0.1902 + 2.952\rho + 37.16\rho^2), \quad (9)$$

$$\frac{E_{c_E}(\rho)}{A} = c_E \times (0.8695 - 17.52\rho - 128.3\rho^2). \quad (10)$$

It is easy to see that $E_{c_D}/A(\rho)$ and $E_{c_E}/A(\rho)$ cancel to a large extent at any density of $0.8 \leq k_F \leq 1.8 \text{ fm}^{-1}$, namely $0.035 \leq \rho \leq 0.394 \text{ fm}^{-3}$, when $c_D \approx 4c_E$ holds. As is shown below, this cancellation persists in the LOBT calculations. The calculations in nuclear matter in Ref. [25] indicate that contributions from the c_D and c_E terms are better to cancel to describe nuclear properties. As far as the nuclear matter energies are concerned, the actual values of c_D and c_E are not important if $c_D \approx 4c_E$. It is even acceptable to set

$c_D = c_E = 0$. Therefore, the main 3NF contributions come from the terms of the coupling constants c_1 , c_3 and c_4 which are settled in the NN sector, though there is a possibility of carefully tuning c_D and c_E in a natural size to achieve a good description of finite nuclei.

B. Results of LOBT calculations

Figure 4 shows saturation curves obtained by the N³LO Ch-EFT NN interaction with the three choices of the cutoff scale: $\Lambda = 450, 550$, and 600 MeV, respectively. The results of the AV18 force [34] shown in Fig. 3 are also included for comparison. As low-energy effective theory, the Ch-EFT potential is not applied to the high momentum region. Hence, the LOBT calculation in Fig. 4 is limited below $k_F = 1.8 \text{ fm}^{-1}$. The Ch-EFT potential with $\Lambda = 550$ MeV is seen to possess a similar saturation property in LOBT to that of AV18. Larger (smaller) cutoff energy affords stronger (weaker) tensor components, and the saturation minimum obeys the Coester band.

When the cutoff scale is small, $\Lambda = 450$ MeV, the tensor component is relatively small and thus the central component gives larger attraction which is not much suppressed by the Pauli blocking. On the other hand, if the attraction provided by the tensor correlation is large in the free space, the attraction is sensitive to the Pauli effect. This explains that the saturation point appears at the lower density with the smaller binding energy. If E/A in fm^{-1} is supposed to scale linearly with k_F in fm^{-1} , saturation minima yield the Coester band.

The results with included the 3NF effects are shown in Fig. 5. The N²LO 3NF V_{123} of the chiral effective field theory is first reduced to an effective NN interaction $V_{12(3)}$ by folding third single-nucleon degrees of freedom.

$$\begin{aligned} & \langle \mathbf{k}'_1 \sigma'_1 \tau'_1, \mathbf{k}'_2 \sigma'_2 \tau'_2 | V_{12(3)} | \mathbf{k}_1 \sigma_1 \tau_1, \mathbf{k}_2 \sigma_2 \tau_2 \rangle_A \\ & \equiv \sum_{\mathbf{k}_3, \sigma_3 \tau_3} \langle \mathbf{k}'_1 \sigma'_1 \tau'_1, \mathbf{k}'_2 \sigma'_2 \tau'_2, \mathbf{k}_3 \sigma_3 \tau_3 | V_{123} | \mathbf{k}_1 \sigma_1 \tau_1, \mathbf{k}_2 \sigma_2 \tau_2, \mathbf{k}_3 \sigma_3 \tau_3 \rangle_A, \end{aligned} \quad (11)$$

where σ and τ denote spin and isospin indices. The density-dependent effective NN force from the N²LO 3NF was first discussed by Holt, Kaiser, and Wesie [24]. Here, the approximation for the off-diagonal matrix elements in their paper is not used. The detailed expressions of the partial wave decomposition are given in Appendices

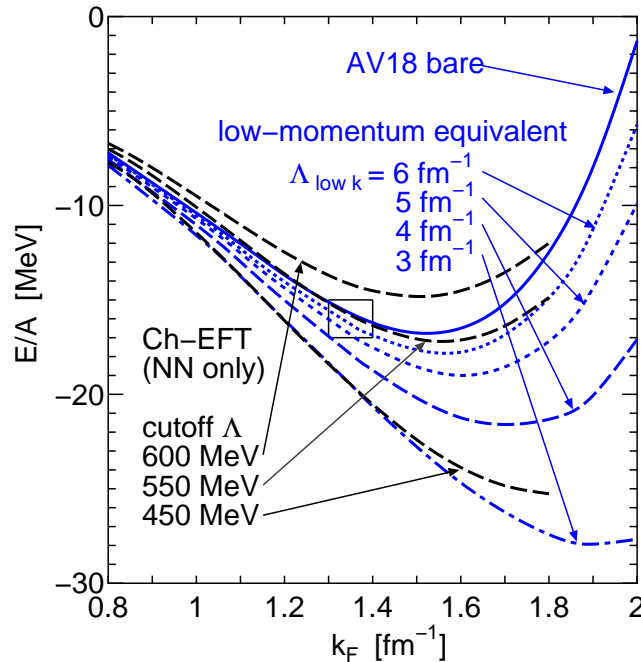


FIG. 4: LOBT saturation curves in symmetric nuclear matter with the continuous choice for intermediate spectra, using the N³LO NN interaction with three choices of the cutoff energy: $\Lambda = 450, 550$, and 600 MeV, respectively. The results of the AV18 force [34] shown in Fig.3 are also plotted for comparison.

of Ref. [25]. When $V_{12(3)}$ is added to the original NN interaction, some caution is necessary for a statistical factor. As is explained in Ref. [25], the following prescription for the G -matrix calculations is used:

$$G_{12} = V_{12} + \frac{1}{3}V_{12(3)} + (V_{12} + \frac{1}{3}V_{12(3)})\frac{Q}{\omega - H}G_{12}. \quad (12)$$

The energies in the propagator are calculated by the single-particle energy defined by

$$e_{\mathbf{k}} = \langle \mathbf{k} | t | \mathbf{k} \rangle + U_G(\mathbf{k}) \quad (13)$$

$$U_G(\mathbf{k}) \equiv \sum_{\mathbf{k}'} \langle \mathbf{k} \mathbf{k}' | G_{12} + \frac{1}{6}V_{12(3)} \left(1 + \frac{Q}{\omega - H} \right) G_{12} | \mathbf{k} \mathbf{k}' \rangle_A. \quad (14)$$

The total energy per nucleon is evaluated as

$$E/A = \frac{1}{\rho} \sum_{\mathbf{k}} \langle \mathbf{k} | t | \mathbf{k} \rangle + \frac{1}{2\rho} \sum_{\mathbf{k}} U_E(\mathbf{k}), \quad (15)$$

where the single-particle potential $U_E(\mathbf{k})$ is different from $U_G(\mathbf{k})$ given above and defined by

$$U_E(\mathbf{k}) = \sum_{\mathbf{k}'} \langle \mathbf{k} \mathbf{k}' | G_{12} | \mathbf{k} \mathbf{k}' \rangle_A. \quad (16)$$

The difference between $U_E(\mathbf{k})$ and $U_G(\mathbf{k})$ may be called a rearrangement contribution of 3NF origin, which is repulsive and of the order of 5 MeV.

Figure 5 shows that when $V_{12(3)}$ is included the cutoff-energy dependence is substantially reduced and the saturation curve is improved to match the empirical one. On the basis of the discussion in the previous subsection, the low-energy constants of the 3NF contact terms are taken to be $c_D = c_E = 0$ as a reference case. The repulsive contribution arises in the 1S_0 state. The net contribution of 3P states is also repulsive, although the attractive spin-orbit interaction is enhanced.

It is helpful to assess the calculated saturation curve by evaluating an incompressibility K , a symmetry energy S and its slope parameter L at the saturation minimum, although it has to be kept in mind that the calculated

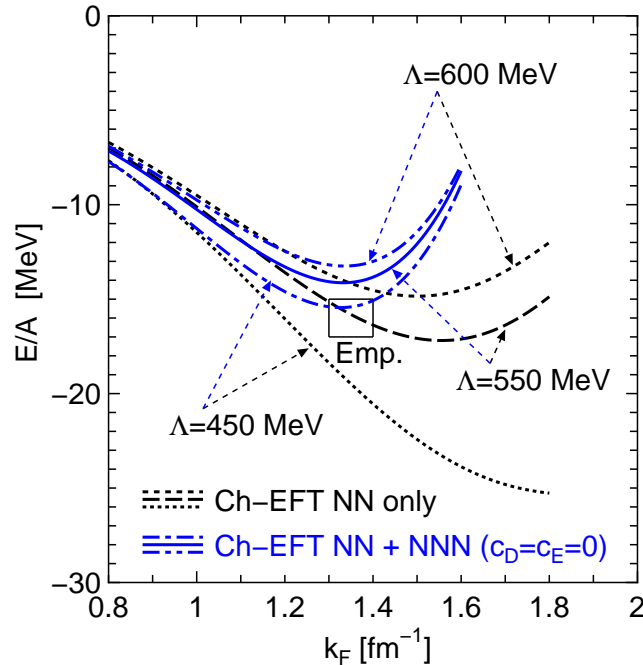


FIG. 5: LOBT saturation curves in symmetric nuclear matter with and without the 3NF effects for three choices of the cutoff energy. The continuous choice is employed for intermediate spectra. The low-energy constants are set as $c_D = c_E = 0$.

TABLE II: Properties of calculated saturation curves in symmetric nuclear matter with $V_{12(3)}$ included in the three cases of the cutoff energy Λ . ρ_0 , K , S , and L are a saturation density, an incompressibility, a symmetry energy, and a slope parameter, respectively.

Λ (MeV)	450	550	600
ρ_0 (fm $^{-3}$)	0.157	0.160	0.162
$E(\rho_0)/A$ (MeV)	-15.4	-14.1	-13.2
K (MeV)	211	209	194
S (MeV)	34	30	30
L (MeV)	70	57	53

curves do not fully reproduce the empirical saturation minimum. The symmetry energy is estimated by the energies of symmetric nuclear matter and pure neutron matter, $E_{SNM}(\rho)/A$ and $E_{PNM}(\rho)/A$; that is, $S = E_{PNM}(\rho_0)/A - E_{SNM}(\rho_0)/A$ where ρ_0 is a saturation density of $E_{SNM}(\rho)/A$, and $L = 3\rho_0 \left. \frac{dE_{PNM}(\rho)/A}{d\rho} \right|_{\rho=\rho_0}$. The saturation curves including the 3NF effects $V_{12(3)}$ shown in Fig.5 correspond to those values given in Table 2.

Let us, now, investigate a range of the changes of the saturation curve due to the different choice of c_D and c_E . Figure 6 shows four cases of the saturation curve; that is, $(c_D = 2.0, c_E = 0)$, $(c_D = -2.0, c_E = 0)$, $(c_D = 0, c_E = 0.5)$, and $(c_D = 0, c_E = -0.5)$, compared with the curve of $(c_D = 0, c_E = 0)$ given in Fig. 5 and that of $(c_D = -4.381, c_E = -1.126)$ in Ref. [25]. It is seen that if $c_D \approx 4c_E$ is satisfied, contributions from the c_D and c_E terms almost cancel also in the LOBT calculations and the saturation curve should be close to that of $c_D = c_E = 0$. It is noted that the absolute value of the c_D and c_E term contributions is smaller than the mean-field value, Eqs. (9) and (10), through the correlation in the G -matrix equation. Another remark is that although the choice of $c_D = c_E = 0$ works well for describing nuclear saturation properties, a different choice within the relation $c_D \approx 4c_E$ might be preferred if a specific spin-isospin character is concerned, because while the c_D term gives rise to a tensor component, the c_E term does not.

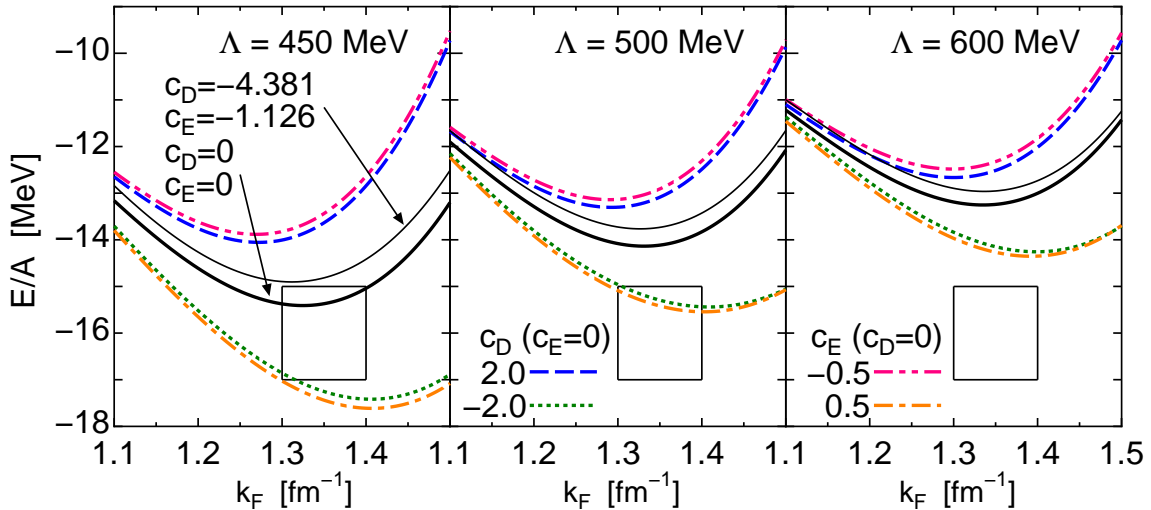


FIG. 6: Dependence of saturation curves on the 3NF low-energy constants c_D and c_E around the reference value of $c_D = c_E = 0$ for the three choices of the cutoff energy Λ . The saturation curves presented in Ref. [25] using $c_D = -4.381$ and $c_E = -1.126$ are also included.

V. QUALITATIVE EXPLANATION OF THE 3NF EFFECTS

It is meaningful to understand, in a qualitative way, the effects of the 3NF in chiral effective field theory; that is, to provide the physical interpretation of the 3NF contributions. The two salient properties are discussed. One is the repulsive effect in the 1S_0 channel, which is basically important to reproduce reasonable saturation properties. The other is the enhancement of the tensor component in the 3S_1 channel. The Pauli blocking plays a central role in both cases. As far as the influence of the 3NF appears dominantly as the Pauli effect, the reduction of the 3NF to an effective two-body interaction in the nuclear medium is justified, because the Pauli effect is operating in two-nucleon processes. It is useful to demonstrate the consequence of these effects by showing, in subsection 5.3, each S and T channel contribution in the potential energy.

A. 1S_0 channel

It has been known that if an isobar Δ excitation in the two-nucleon scattering process is explicitly considered, the contribution of the diagram depicted in Fig. 7(a) supplies the $(NN)_{L=0,S=0,J=0}$ state being caused by the tensor component of the pion exchange, the attraction is similar to that of the tensor correlation in the 3S_1 channel. When the 1S_0 interaction is embedded in the nuclear medium, the excitation to the (ΔN) intermediate state is partly Pauli-blocked, Fig. 7(b). The suppression of the attraction leads to the repulsive effect. This mechanism has been studied by various authors. It is also known that the Pauli-blocking effect for the Δ -excitation can be described by introducing 3-body interaction of the Fujita-Miyazawa type, Fig. 7(c).

In the description of NN interaction in chiral effective field theory, the isobar Δ -excitation does not explicitly appear in most cases. Its effects are certainly inherent in the coupling constants. The 3NF involving these coupling constants brings about the relevant Pauli blocking effect.

B. 3S_1 channel

The mechanism discussed in Sect. 3-1 is irrelevant in the 3S_1 channel because of the isospin. There is, however, another Pauli blocking effect for the tensor component of the 3S_1 NN interaction. The strong tensor force arising from the one-pion exchange is one of the most salient features of the NN interaction. In the actual construction of the NN interaction in the one-boson exchange potential (OBEP) model, the one-pion exchange tensor component has to be weakened to fit the scattering data. One plausible natural mechanism is the cancellation by the tensor component of the ρ -meson exchange in the opposite sign. In the Ch-EFT, the ρ -meson is irrelevant. However, the reduction of the one-pion exchange tensor component is found to be given [46] by the two-pion exchange process, Fig. 8(a). As in the same way for the Δ -excitation, this process is partly Pauli-blocked in the nuclear medium, Fig. 8(b), and the effect is taken into account by considering the 3NF, Fig. 8(c). The suppression of the two-pion exchange process means that the tensor force is enhanced in the 3S_1 channel in the nuclear medium, depending on the density of nuclear matter, compared with that in the free space. This enhancement of the tensor component is not expected in the standard OBEP picture. On the other hand, it has been known that two-pion exchange 3NFs effectively strengthen the two-nucleon tensor force.

In order to quantify the 3NF effects for the strength of the tensor component in nuclear matter at the normal density, the bare diagonal matrix elements of the S-D tensor interaction and those in low-momentum space are shown in Fig. 9 with and without 3NFs for the 3 cases of the cutoff mass $\Lambda = 450, 550$, and 600 MeV,

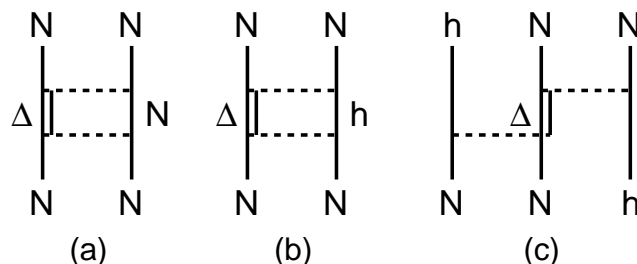


FIG. 7: Diagrams including isobar Δ excitation: (a) a process to be implicitly taken into account in the description of NN interaction, (b) "h" standing for an occupied state, and (c) a 3NF diagram of the Fujita-Miyazawa type.

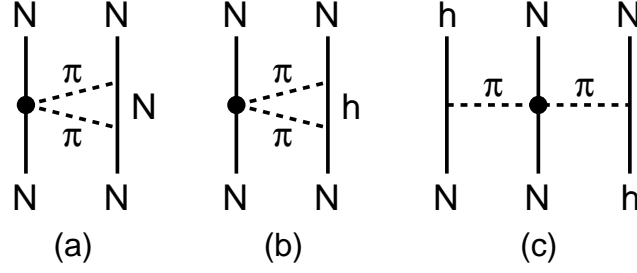


FIG. 8: Two-pion exchange diagrams: (a) a process taken into account in the description of NN interaction in Ch-EFT, (b) "h" standing for an occupied state, and (c) a 3NF diagram in Ch-EFT.

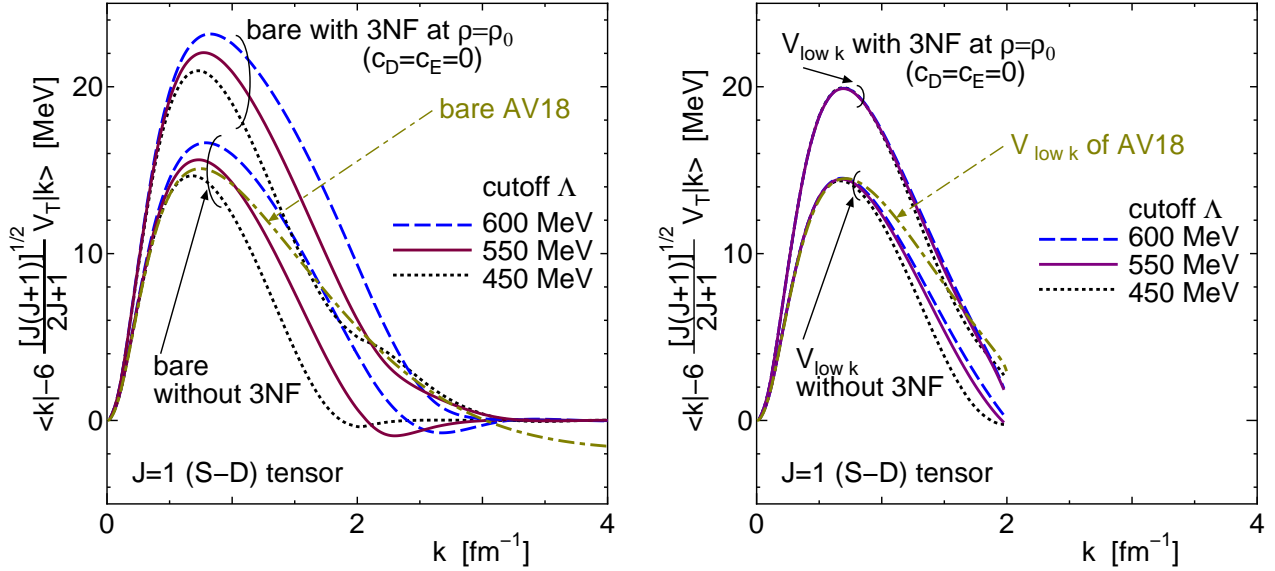


FIG. 9: S-D tensor diagonal matrix element in momentum space. The left panel is for the bare interaction with and without $V_{12(3)}$ for the three cases of the cutoff energy Λ . The right panel is for the low-momentum equivalent interaction with $\Lambda_{lowk} = 2$ fm⁻¹.

respectively. Figure 9 is for the case of $c_D = c_E = 0$. It is seen that the magnitude of the bare S-D tensor interaction is enhanced by about 40 % at the normal density through the 3NF, and this influence remains in low-momentum space with $\Lambda_{lowk} = 2$ fm⁻¹. It is interesting that the two-body tensor interactions with the different cutoff Λ become almost identical when they are transformed into low-momentum space, though the difference is apparent in bare matrix elements. It is noteworthy that this collapse holds even after 3NF effects are included. Namely, the equivalent tensor force in low-momentum space is insensitive to the cutoff scale Λ .

As noted at the end of the subsection 4.2, the tensor component is brought about through the c_D term. Figure 10 compares the bare and low-momentum diagonal S-D matrix elements with ($c_D = c_E = 0$) and those with ($c_D = -4.381$, $c_E = -1.126$) used in Ref. [25]. In the latter case, the enhancement of the magnitude of the S-D tensor interaction is seen to become smaller to be about 30 %, which indicates the quantitative effect of the c_D term of the 3NF to the effective tensor force.

The enhancement of the effective tensor interaction in the nuclear medium due to the 3NF might be checked by some adequate experimental observables. The enhanced tensor interaction of the NN interaction in the nuclear medium brings about larger attraction in the 3S_1 channel through the tensor correlation. For the nucleon in scattering states, it makes the imaginary part of the optical potential larger. This effect may be examined by considering nucleon-nucleus and nucleus-nucleus scattering processes. Promising results are reported in Refs. [47, 48].

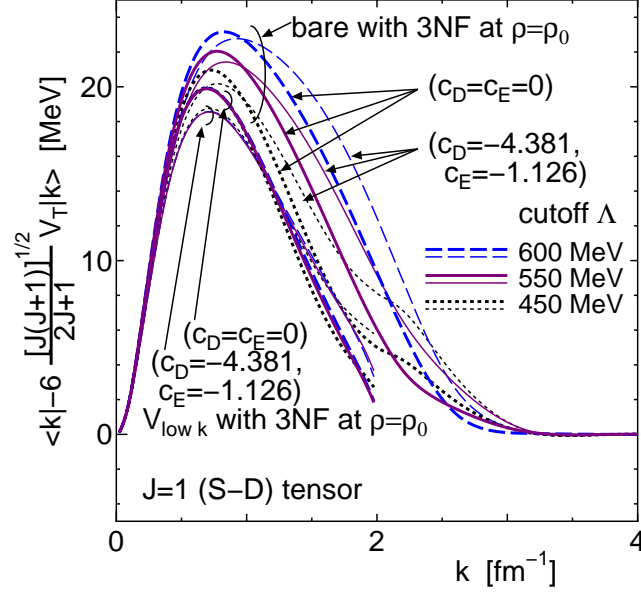


FIG. 10: Comparison of bare and low-momentum S-D tensor diagonal matrix elements in momentum space for the two choices of c_D and c_E parameters: $(c_D = c_E = 0)$ and $(c_D = -4.381, c_E = -1.126)$. Three cases of the cutoff energy Λ are shown. The low-momentum cutoff is $\Lambda_{low k} = 2 \text{ fm}^{-1}$. Note that the curves of the different cutoff energy Λ for the low-momentum space are virtually indistinguishable.

C. Each S - T channel contribution of the potential energy

Summarizing the effects discussed in the preceding subsections, each of ^1O , ^3E , ^1E , and ^3O contributions in the potential energy in nuclear matter is given in Fig. 11 in the case of the cutoff $\Lambda = 550$. The corresponding energy obtained by the Gogny D1S density-dependent effective interaction [49], which has been commonly used for a mean-field description of finite nuclei, is included.

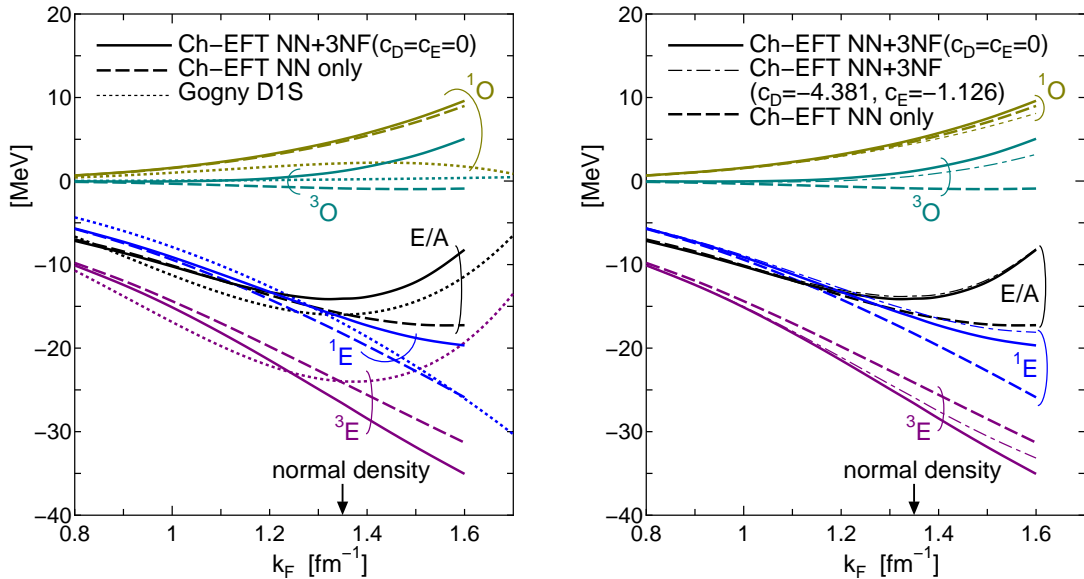


FIG. 11: Decomposition of the potential energy to ^1O , ^3E , ^1E , and ^3O contributions in the case of $\lambda = 550$ MeV. The left panel is a comparison of the results with and without 3NF contributions for $c_D = c_E = 0$. The results from the Gogny D1S density-dependent effective interaction [49] are also shown. The right panel includes, in addition, the results with $c_D = -4.381$ and $c_E = -1.126$.

The difference between the solid and the dashed curves indicates the effect of the 3NF. The repulsive contribution in the ^3O channel as well as in the ^1E channel is responsible for bringing the saturation minimum at the lower density. The ^1O channel is scarcely affected by the 3NF. The largest attractive contribution in the ^3E channel increases through the enhanced tensor component, as discussed in the subsection 3.2. The knowledge of these 3NF contributions may be used to improve the properties of phenomenological effective interactions. It is interesting to see that the results of the Ch-EFT interaction with the 3NF effects are similar to those of the Gogny D1S interaction below the normal density. It is not surprising that the D1S curves deviates from those of the Ch-EFT at higher density regions, because the spin-dependent character of the density dependent part is not well controlled by the data of finite nuclei. While the saturation is assured by the density-dependent term in the ^3E channel in the description of D1S, it is brought about by the repulsion appeared in the ^1E and ^3O channels in the Ch-EFT description.

VI. SUMMARY AND REMARKS

The saturation mechanism of nuclear matter has been discussed in view of chiral effective field theory, in which three-nucleon interactions consistent with the two-nucleon part are systematically defined. The uncertainties of nuclear matter calculations in the lowest-order Brueckner theory, which has been known as the Coester band, were revisited employing modern NN potentials and their low-momentum equivalent interactions. Then, the results using the chiral N^3LO NN and N^2LO 3N potentials with the three choices of cutoff parameters, $\Lambda = 450, 550, \text{ and } 600$ MeV, are presented. As effective theory, the predictions for empirical quantities are desirable not to depend on the cutoff scale of the parameterization. The effective parameters fitted in the two-nucleon interaction level vary depending on the different cutoff energy, which naturally bear different off-shell properties, and they are related each other by some unitary transformation. Therefore, as was shown in Sections 2 and 3, the nuclear matter saturation point in the LOBT moves on the Coester band depending on the cutoff energy.

It is noteworthy to see that the inclusion of the 3NF changes the situation and the nuclear saturation is reasonably well reproduced after the 3NF effects are incorporated. The 3NFs are treated by reducing them to effective two-body interactions by folding the third nucleon degrees of freedom. As explained in the discussion of Sec. 5, this approximation is justified by the fact that the main effects of the 3NF can be regarded as resulting from the inclusion of the Pauli effects in two-pion exchange processes of the two-nucleon interaction. It is to be noted that the contributions of the specific 3NF processes bearing new parameters c_D and c_E , turn out to give minor effects, as far as the relation $c_D \approx 4c_E$ is satisfied. The prescription of $c_D \approx 4c_E$ is favorable for explaining nuclear saturation properties in the LOBT. Thus, calculations using $c_D = c_E = 0$ are mainly presented as a reference case. Then, the dependence of the calculated result on the choice of c_D and c_E is shown. If a specific component of the effective NN interaction in the nuclear medium is interested, fine tuning of c_D and c_E may be applied. Except for the reasonable choice of c_D and c_E , being in a natural size, no adjustable parameter is introduced in this paper.

The repulsive contribution in the 1S_0 state is understood as the effect of the suppression of the isobar Δ excitation in the nuclear medium, which has been known a long time, although there is no explicit Δ in the present N^3LO interaction. In the 3S_1 channel, the isobar Δ is irrelevant. In this case, the important effect appears through the tensor component. The one-pion exchange has a strong tensor component. To match the experiment, the strength is needed to be reduced. A physical and natural cut is provided, with a description of a OBEP model, by the ρ -meson exchange which has a tensor component in the opposite sign. In chiral effective theory, a two-pion exchange process replace the role of the ρ -meson exchange, and the two-pion exchange is hindered in the nuclear medium to partly restore the one-pion exchange tensor component.

The significant role of the 3NF in realizing correct nuclear saturation properties indicates that other baryon degrees of freedom than protons and neutrons, which are eliminated in constructing potential description, are important. The 3NF is analogous to the appearance of induced many-body interactions in a restricted space of nuclear many-body theory. Though the reason of justifying the reduction of the 3NFs to an effective two-nucleon interaction in the medium is explained, it is certain that a full treatment of the 3NF is necessary. Concerning this problem, it is noted as a final remark that the wound integral κ of the LOBT calculation with the Ch-EFT potential is somewhat large, in particular when the 3NF effects are included, $\kappa \simeq 0.25$, compared to that of other modern NN potentials which is around $\kappa \simeq 0.15$. This suggests that the convergence of the Brueckner-Bethe-Goldstone hole-line expansion is slower. It is therefore important in the future to quantitatively estimate more than three-nucleon correlation energies in the nuclear medium using the Ch-EFT interaction.

Acknowledgment

This work is supported by the Japan Society for the Promotion of Science (JSPS) KAKENHI Grant No. 25400266.

-
- [1] H. Yukawa, Proc. Physico-Mathematical Society of Japan, **17**, 48 (1935).
 - [2] K.A. Brueckner, C.A. Levinson, and H.M. Mahmoud, Phys. Rev. **95**, 217 (1954).
 - [3] J. Goldstone, Proc. Roy. Soc. **A239**, 267 (1957).
 - [4] B.D. Day, Rev. Mod. Phys. **39**, 719 (1967).
 - [5] H.A. Bethe, Ann. Rev. Nucl. Sci. **21**, 93 (1971).
 - [6] B.D. Day, Rev. Mod. Phys. **50**, 495 (1978).
 - [7] Z.H. Li, U. Lombardo, H.-J. Schulze, W. Zuo, L.W. Chen, and H.R. Ma, Phys. Rev. **C74**, 047304 (2006).
 - [8] H.Q. Song, M. Baldo, G. Giansiracusa, and U. Lombardo, Phys. Rev. Lett. **81**, 1584 (1998).
 - [9] V.R. Pandharipande and R.B. Wiringa, Rev. Mod. Phys. **51**, 821 (1979).
 - [10] M. Baldo and G.F. Burgio, Rep. Prog. Phys. **75**, 026301 (2012).
 - [11] J. Fujita and H. Miyazawa, Prog. Theor. Phys. **17**, 366 (1957).
 - [12] R. Brockmann and R. Machleidt, Phys. Rev. C **42**, 1965 (1990).
 - [13] G.E. Brown and A.M. Green, Nucl. Phys. A **137**, 1 (1969).
 - [14] B.A. Loiseau, Y. Nogami, and C.K. Ross, Nucl. Phys. A **165**, 601 (1971); Erratum A **176**, 665 (1971).
 - [15] T. Kasahara, Y. Akaishi, and H. Tanaka, Prog. Theor. Phys. Suppl. **56**, 96 (1974).
 - [16] B. Friedman and V.R. Pandharipande, Nucl. Phys. A **361**, 361 (1981).
 - [17] E. Epelbaum, H.-W. Hammer, and U.-G. Meißner, Rev. Mod. Phys. **81**, 1773 (2009).
 - [18] R. Machleidt and D.R. Entem, Phys. Rep. **503**, 1 (2011).
 - [19] S.K. Bogner, A. Schwenk, R.J. Furnstahl, and A. Nogga, Nucl. Phys. A **763**, 59 (2005).
 - [20] K. Hebeler and A. Schwenk, Phys. Rev. C **82**, 014314 (2010).
 - [21] K. Hebeler, S.K. Bogner, R.J. Furnstahl, A. Nogga, and A. Schwenk, Phys. Rev. C **83**, 031301(R) (2011).
 - [22] L. Coraggio, J.W. Holt, N. Itaco, R. Machleidt, L.E. Marcucci and F. Sammarruca, Phys. Rev. C **89**, 044321 (2014).
 - [23] M. Kohno, Phys. Rev. C **86**, 061301(R) (2012).
 - [24] J.W. Holt, N. Kaiser, and W. Weise, Phys. Rev. C **81**, 024002 (2010).
 - [25] M. Kohno, Phys. Rev. C **88**, 064005 (2013).
 - [26] F. Sammarruca, B. Chen, L. Coraggio, N. Itaco, and R. Machleidt, Phys. Rev. C **86**, 054317 (2012).
 - [27] F. Sammarruca, L. Coraggio, J. W. Holt, N. Itaco, R. Machleidt, and L. E. Marcucci, Phys. Rev. C **91**, 054311 (2015).
 - [28] A. Carbone, A. Cipollone, C. Barbieri, A. Rios, and A. Polls, Phys. Rev. C **88**, 054326 (2013).
 - [29] A. Carbone, A. Rios, and A. Polls, Phys. Rev. C **90**, 054322 (2014).
 - [30] S. K. Bogner, T. T. S. Kuo, and A. Schwenk, Phys. Rep. **386**, 1 (2003).
 - [31] F. Coester, S. Cohen, B. Day, and C.M. Vincent, Phys. Rev. C **1**, 769 (1970).
 - [32] E. Schiller, H. Müther, and P. Czerski, Phys. Rev. C **59**, 2934 (1999); **60**, 059901 (1999).
 - [33] K. Suzuki, R. Okamoto, M. Kohno, and S. Nagata, Nucl. Phys. A **665**, 92 (2000).
 - [34] R.B. Wiringa, V.G.J. Stoks, and R. Schiavilla, Phys. Rev. C **51**, 38 (1995).
 - [35] T. A. Rijken, V. G. J. Stoks, and Y. Yamamoto, Phys. Rev. C **59**, 21 (1999).
 - [36] R. Machleidt, Phys. Rev. C **63**, 024001 (2001).
 - [37] Y. Fujiwara, Y. Suzuki, and C. Nakamoto, Prog. Part. Nucl. Phys. **58**, 439 (2007).
 - [38] K. Suzuki and S. Y. Lee, Prog. Theor. Phys. **64**, 2091 (1980).
 - [39] S. Y. Lee and K. Suzuki, Phys. Lett. **B91**, 173 (1980).
 - [40] J. Kuckei, F. Montani, H. Müther, and A. Sedrakian, Nucl. Phys. **A723**, 32 (2003).
 - [41] E.D. Jurgenson, P. Navrátil, and R.J. Furnstahl, Phys. Rev. **C83**, 034301 (2011).
 - [42] K. Suzuki, R. Okamoto, and Kumagai, Phys. Rev. **C36**, 804 (1987).
 - [43] S. Fujii, R. Okamoto, and K. Suzuki, Phys. Rev. Lett. **103**, 182501 (2009).
 - [44] E. Epelbaum, W. Götke, and U.-G. Meißner, Nucl. Phys. A **747**, 362 (2005).
 - [45] P. Navrátil, V.G. Gueorguiev, J.P. Vary, W.E. Ormand, and A. Nogga, Phys. Rev. Lett. **99**, 042501 (2007).
 - [46] N. Kaiser, R. Brockmann, and W. Weise, Nucl. Phys. A **625**, 758 (1997).
 - [47] M. Toyokawa, K. Minomo, M. Kohno, and M. Yahiro, J. Phys. G: Nucl. Part. Phys. **42**, 025104 (2015).
 - [48] K. Minomo, M. Toyokawa, M. Kohno, and M. Yahiro, Phys. Rev. **C90**, 051601(R) (2014).
 - [49] J. F. Berger, M. Girod, and D. Gogny, Comput. Phys. Commun. **63**, 365 (1991).